PROCEEDINGS OF SPIE

SPIEDigitalLibrary.org/conference-proceedings-of-spie

Localized surface plasmons on periodic monolayer black phosphorene nanoribbons tuned in the infrared region with a dielectric substrate

Oluwatobi Olorunsola, Desalegn T. Debu, David French, Stephen J. Bauman, Joseph B. Herzog

Oluwatobi Olorunsola, Desalegn T. Debu, David French, Stephen J. Bauman, Joseph B. Herzog, "Localized surface plasmons on periodic monolayer black phosphorene nanoribbons tuned in the infrared region with a dielectric substrate," Proc. SPIE 10722, Plasmonics: Design, Materials, Fabrication, Characterization, and Applications XVI, 107222R (19 September 2018); doi: 10.1117/12.2321339

SPIE.

Event: SPIE Nanoscience + Engineering, 2018, San Diego, California, United States

Localized surface plasmons on periodic monolayer black phosphorene nanoribbons tuned in the infrared region with a dielectric substrate

Oluwatobi Olorunsola[a], Desalegn T. Debu[b], David French[b], Stephen J. Bauman[a], Joseph B. Herzog[a,b,c]

[a]Microelectronics-Photonics Program, University of Arkansas, Fayetteville, AR, 72701, USA;
[b]Department of Physics, University of Arkansas, Fayetteville, AR, 72701, USA;
[c]R.B. Annis School of Engineering, University of Indianapolis, Indianapolis, IN 46227

ABSTRACT

Localized surface plasmons have been reported for periodic 2D monolayer black phosphorene (BP) nanoribbons in the infrared region. The anisotropic nature of BP causes different plasmonic effects depending on their orientation over select dielectric substrates, leading to tunability and promising future applications in imaging and other detectors. Computational models are used to demonstrate that by tuning the localized plasmonic resonance, as well as the orientation of the BP nanoribbon, it is possible to obtain desired coupled resonance modes and enhanced absorption capabilities. The modes obtained from the absorption spectra span the infrared range and extend our understanding of BP plasmons.

Keywords: Black Phosphorene, Plasmonic Enhancement, 2D Materials

1. INTRODUCTION

Light-matter interactions in atomically-thin noble metal films and two-dimensional (2D) materials such as graphene and black phosphorous (BP) have gained wide-spread prominence in nanophotonic, optoelectronic, and photovoltaic research and applications. While noble metal films have been identified as excellent candidates for strong surface plasmonic confinement, leading to enhanced absorption capabilities and Raman scattering, these sufficiently strengthened fields are limited to the ultraviolet (UV) through near-infrared (NIR) spectral range. Beyond this spectral range, plasmonic field responses are weak, with narrow spectral resonances owing to high negative permittivity,[1] and they are subverted by limited tunability due to high losses.[2-3]

In contrast, graphene is an exceptional 2D material with a reputation for its high carrier mobility and unique band structure, which lead to low attenuation of surface plasmon resonance. These plasmons typically manifest in the mid-IR and low terahertz spectral ranges through a wide variety of tuning strategies achieved experimentally by either increasing doping levels, reduced structural dimensions, or gate modulation.[4-7] In addition to graphene, black phosphorous, an emerging 2D material with a 2-dimensional puckered hexagonal honeycomb structure, has been noticed in the scientific community as a potential candidate for applications where strong light-matter interactions are involved.[8-13] In contrast to graphene, BP surface plasmons reveal exotic properties that feature dependence on polarization and the size of the monolayer[14-17], as well as a potential for long range disorder[18]. These properties are attributed to its strong in-plane anisotropic electronic and optical properties as well as high mobility and a tunable direct bandgap.[19-21] These desirable capabilities also make BP a potential candidate for use in hyperspectral imaging applications and silicon photonics.[25-28] Unfortunately, incorporation of BP into current technologies has been limited to few applications due to its instability in ambient conditions.[26-31] Here, we discuss BP as alternative material to graphene and other films, while addressing limitations posed by metals and 2D graphene for surface plasmons in the mid-to-far infrared spectral range. Finally, we explore, based on our previous work[43] the strategies for minimizing oxidation drawbacks with the aim to maintain edge-plasmon absorption.

Plasmonics: Design, Materials, Fabrication, Characterization, and Applications XVI, edited by Din Ping Tsai, Takuo Tanaka, Proc. of SPIE Vol. 10722, 107222R · © 2018 SPIE
CCC code: 0277-786X/18/$18 · doi: 10.1117/12.2321339

2. MODEL

We employ the semiclassical Drude model (Eq. 1) for a full description of the photonic properties of the 2D BP anisotropic layer.[14] Here, ε_{jj} represents the permittivity along the so-called armchair (x) and zigzag (y) directions.

$$\varepsilon_{jj} = \varepsilon_r + \frac{i\sigma_{jj}}{\omega\varepsilon_0 t_{BP}} \tag{1}$$

Constants ε_r = 5.65[31] and t_{BP} = 0.7nm[20] represent the relative permittivity and thickness of the anisotropic BP monolayer, ω is the angular frequency of the incident light, and σ_{jj} represents associated local surface conductivity given as:

$$\sigma_{jj} = \frac{i\hbar D_j}{\pi(\hbar\omega + i\eta)} \tag{2}$$

where $\hbar$ is the reduced Planck constant. The parameter η describes the scattering rate and is chosen to be 10 meV to account for damping effects.[14] $D_j = \pi n e^2/m_j$ is the Drude weight and is related to the anisotropic effective electron mass, m_j, and N is the electron density. The effective electron mass along the armchair and zigzag directions are $m_{cx} = \hbar^2/\left(\frac{2\gamma^2}{\Delta} + \eta_c\right)$ and $m_{cy} = \hbar^2/2v_c$, respectively.[14,32] The conduction band parameters for monolayer BP are given as $\eta_c = \hbar^2/0.4m_0$, $v_c = \hbar^2/1.4m_0$, with m_0 as the electron mass, bandgap $\Delta = 2eV$, and $\gamma = 4\,a/\pi\ eVm$, where $a = 0.223\,nm$ and π/a is the width of the Brillouin Zone in the x-direction.[14,32]

3. RESULT AND ANALYSIS

A 3D schematic representation of the structure designed to investigate the surface plasmon polaritons (SPPs) on periodic BP nanoribbons is shown in Fig. 1a, with a corresponding cross-sectional 2D view of a single period depicted in Fig. 1b. Periodic arrays of BP ribbons are simulated as spatially situated in the *x*-*y* plane (z = 0). An optically thick gold layer with reflective capability is added to the model to confine enhanced light. The nanoribbons are separated from the gold reflector surface by a dielectric layer of refractive index n_2, (z < 0). A dielectric medium of refractive index n_1 tops the BP periodic nanoribbon array (z > 0). Wavelength-dependent optical constants of gold are obtained from Palick et al.[33]

Fig. 1(c-d) shows the electric field intensity distribution obtained from a finite element simulation[34] for illumination via plane waves at two different wavelengths. The geometrical parameters used in the simulation are as follows: the width (w) of the BP nanoribbon is 150 nm, the period is 250 nm, while the gap which makes up the difference between the width and the period is set to 100 nm. The values of the BP ribbon width were chosen to accommodate tunable range reach in the far-IR region of the EM spectrum. The dielectric substrate (n_2 = 1.71) of thickness 5μm sits beneath the modeled ribbon, which is surrounded by air (n_1 = 1.00). In 2D structures, it can be inferred that strong field enhancement and localization of plasmonic modes can create enhanced spectral absorption conditional on the nature and shape of the surrounding dielectric structure.[35,43]

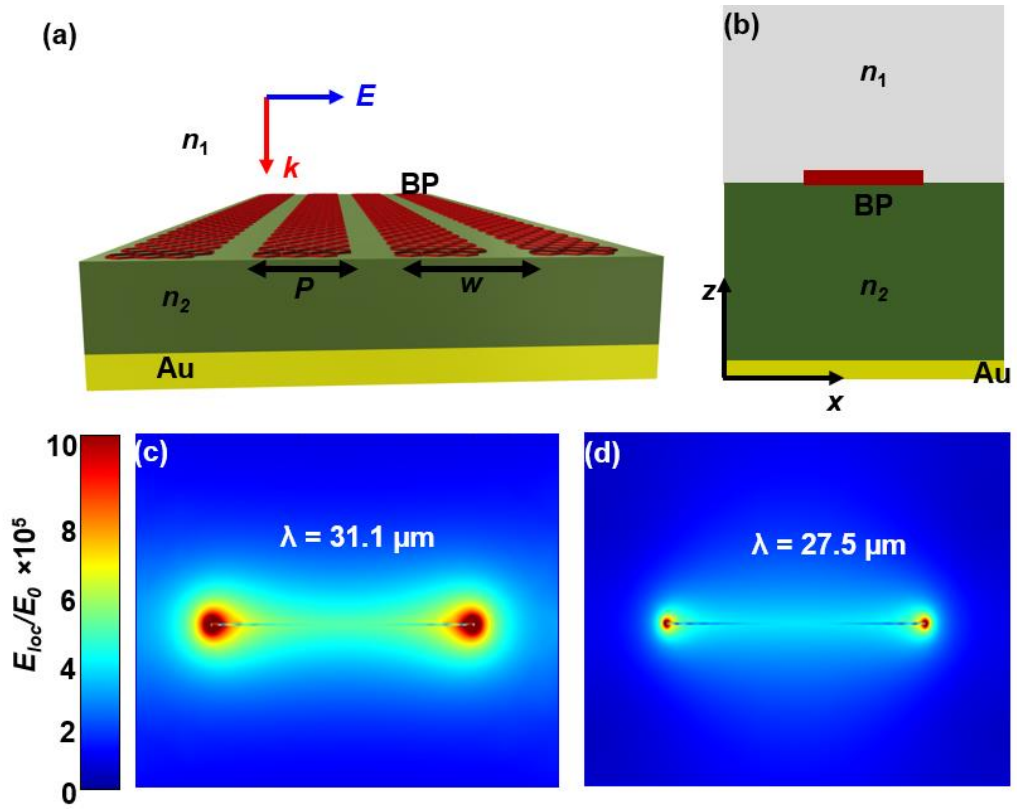

Fig. 1: Simulated results of the EM response of the illuminated BP **(a)** 3D Schematic of periodic phosphorene nanoribbons on dielectric surface (green) atop a gold reflective structure **(b)** 2D cross-sectional view of **(a)** with BP, gold beneath two dielectric layers, n_1 and n_2, with *E* and *k* labeled as light polarization and propagation directions, respectively. **(c-d)** Computed electric field enhancement distributions. Parameters used in the model are as follows: w = 15nm, P = 250nm, n_1 = 1.0, and n_2 = 1.71, N = 10^{-13} cm^{-2}, at λ = (c) 31.1, (d) 27.5 μm.

Based on the simulation results, the computed normal-incidence absorption response (Fig. 2a) is shown for the BP nanoribbons (w = 150nm and P = 25nm). In this case, the refractive index n_1 was kept constant while the absorptive medium n_2 sweeps over a wide range of material indices. The materials simulated are sapphire (1.71)[36], potassium bromide (1.43) [37], polymethyl methacrylate (1.45) [38], polystyrene (1.50) [38] and silicon (3.32) [33]. The absorption peak resonant wavelength is plotted against the refractive index n_2 as seen in Fig. 2(b). It is found that as n_2 increases, the absorption peak response broadens and shifts to higher infrared wavelengths and is consistent with both theory and simulation. Under normal incidence of light, the analytical solution of the resonant peak wavelength is based on the grating model and obtained by:

$$\lambda_p = \pi c \sqrt{\frac{2P\varepsilon_0(\varepsilon_1+\varepsilon_2)m_j}{m\pi N e^2}} \tag{3}$$

where λ_p is the resonance wavelength of BP plasmons, P is the period of the grating, c is the speed of light, e is the charge of an electron, ε_0 is the permittivity of free space, and m is a positive integer and is represented as the order of the dispersion of the confinement diffraction. Coupling effects introduced by the plasmonic waves between neighboring BP nanoribbons as well as anomalous reflections associated with two nanoribbon edges can cause the reflected plasmons to create an interference effect that incorporates a new phase factor other than π. The reflected waves between the nanoribbon edges create constructive interference with the surface plasmons, thus satisfying the criteria $2wRe(k_{z1}) + 2\phi = 2m\pi$[39-40] where w is the nanoribbon width, ϕ represents the phase of the edge reflected wave, and m is the peak resonance order. Analytical estimates of ϕ are obtained by fitting the simulated results of the nanoribbon surrounded by select dielectric structures

following Eq. 4. Using Eq. 4, theoretical and simulation estimates are calculated for the resonant absorption wavelengths for varying refractive indices, n_2.

$$\frac{\phi}{\pi} = m - \frac{\varepsilon_0(\varepsilon_1+\varepsilon_2)}{D_{xx}}\left(\frac{2\pi c}{\lambda_p}\right)^2 \quad (4)$$

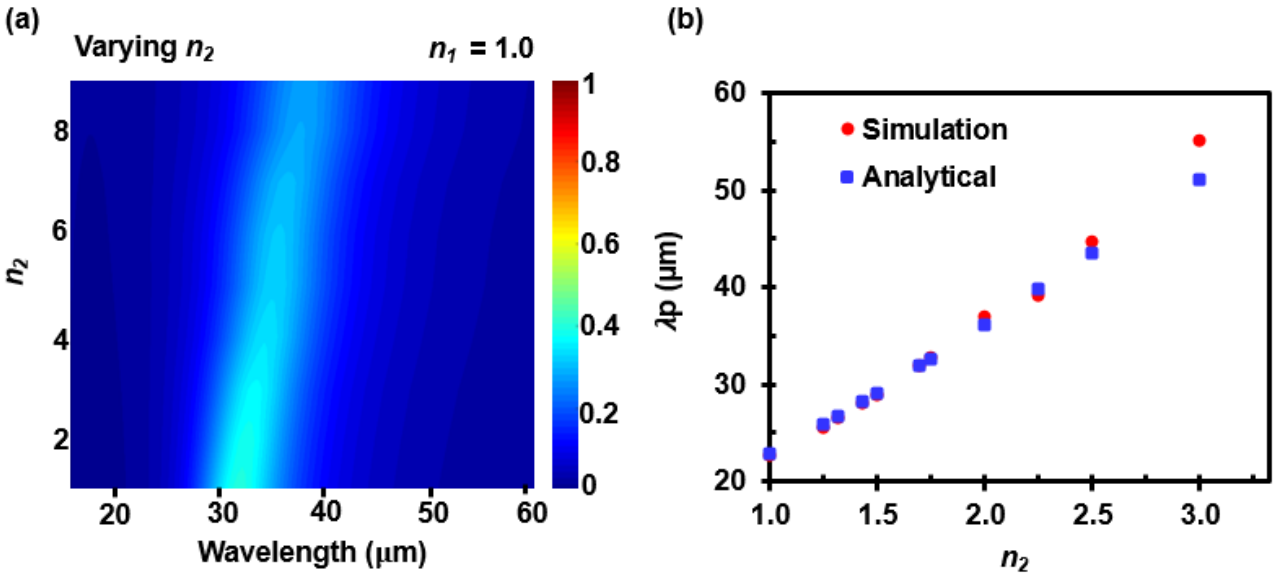

Fig. 2: Effects of changing n_2 on absorption response with n_1 held constant (a) Color map showing computed normal-incidence TM mode electric field absorption response for BP periodic nanoribbons in air (n_1 = 1.0) under different substrates with refractive indices n_2. (b) Fundamental mode (m = 1) of the absorption peak resonant wavelength as a function of the refractive index of the dielectric substrate n_2. The red dots are derived from the finite-element method (FEM) model while the blue squares are obtained from the theoretical model explained in Eq. 4.

4. ABSORPTION ENHANCEMENTS

According to our theoretical model, plasmonic resonance and enhanced absorptions should depend on the anisotropic effective mass which is related to the BP layer thickness and the electron carrier density. From Eq.4, it is apparent that decreasing the effective mass causes a blue shift and strong plasmon localizations, while a red shift occurs by decreasing the electron carrier density (related to the carrier mobility) [41-42]. To achieve tunability of plasmon resonances as well as absorption capabilities in BP ribbons, it is important to study the implications of modifying the ribbon geometry as well as the conductivity.

Figure 3(a-b) shows the armchair and zigzag polarization directions of the BP monolayer ribbons. The aim is to significantly improve the absorption in both directions. Using Eq. 4, it is possible to tune the absorption intensity by modifying the width of the nanoribbons as well as the number density. For a quantitative inspection of this tuning effect, absorption intensity plots were obtained for both armchair and zigzag polarization directions. Parameters used in the absorption simulation model are as follows: P = 250nm, held constant over ribbon width from 100 to 225nm, number density N = 2.5 x 10^{13}cm^{-2} , with n_1 = 1.0 and n_2 = 1.71.

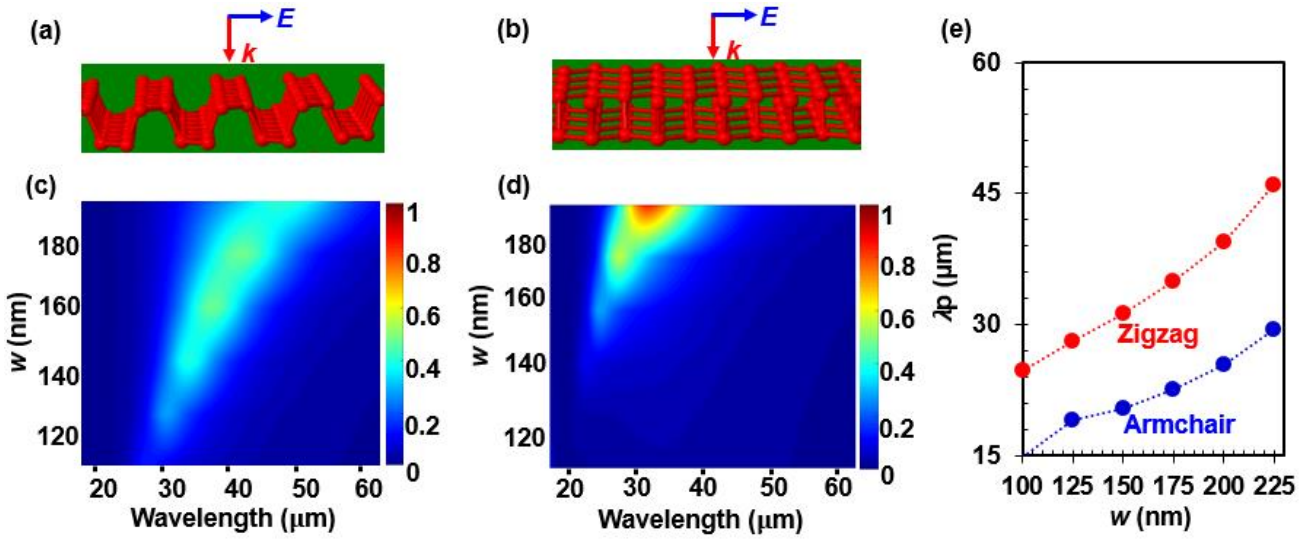

Fig. 3: Optical responses are compared for atomic structure of monolayer BP in the (a) Armchair (b) zigzag polarization directions. Results from simulations are obtained for absorption responses for normal-incidence TM-mode light along the (c) Armchair (d) zigzag direction for different widths, w(nm). In this case, n_2= 1.71, n_1= 1.0, N = 2.5 x 10^{13}cm^{-2}, and P = 250nm. (e) Absorption peaks with respect to the width for both armchair and zigzag polarization directions.

Fig. 3 (a-e) compares the optical responses of polarized light in both armchair and zigzag directions. It is seen that the absorption peak wavelength is largely influenced by the nanoribbon width and can be explained by the resonance conditions of the localized surface plasmon. Additionally, due to the weak plasmon confinement in the armchair direction, absorption strength is minimal (Fig 3c). From Fig. 3e, we infer[43] that the width is an important parameter for tuning capabilities in BP plasmonic behaviors for both the armchair and zigzag polarization directions. For the same values of *w*, the difference in the wavelength peak values between these two orientations is due to different anisotropic masses, resulting in two imaginary dielectric functions.

5. SHIELDING NANORIBBON

Periodic BP nanoribbons are highly susceptible to effects of exposure to oxygen and moisture which often result in structural distortions and the formation of porous regions[14]. To mitigate degradation through oxidation, a protective nanolayer of anisotropic hexagonal boron nitride (hBN) metamaterial was introduced to encapsulate the BP ribbons. Besides acting as a protective layer for the BP ribbons, the hBN is also responsible for providing chemical inertness, high mechanical strength, and high thermal resilience.[41,42] Figure 4 (a-b) shows the incorporation of different hBN layer thicknesses, *d*, to our initial simulation design (Fig. 1). The armchair and zigzag polarization directions are also displayed. Additionally, simulation results are shown for the TM electric field absorption responses with thickness *d* swept from 0 to 10nm.

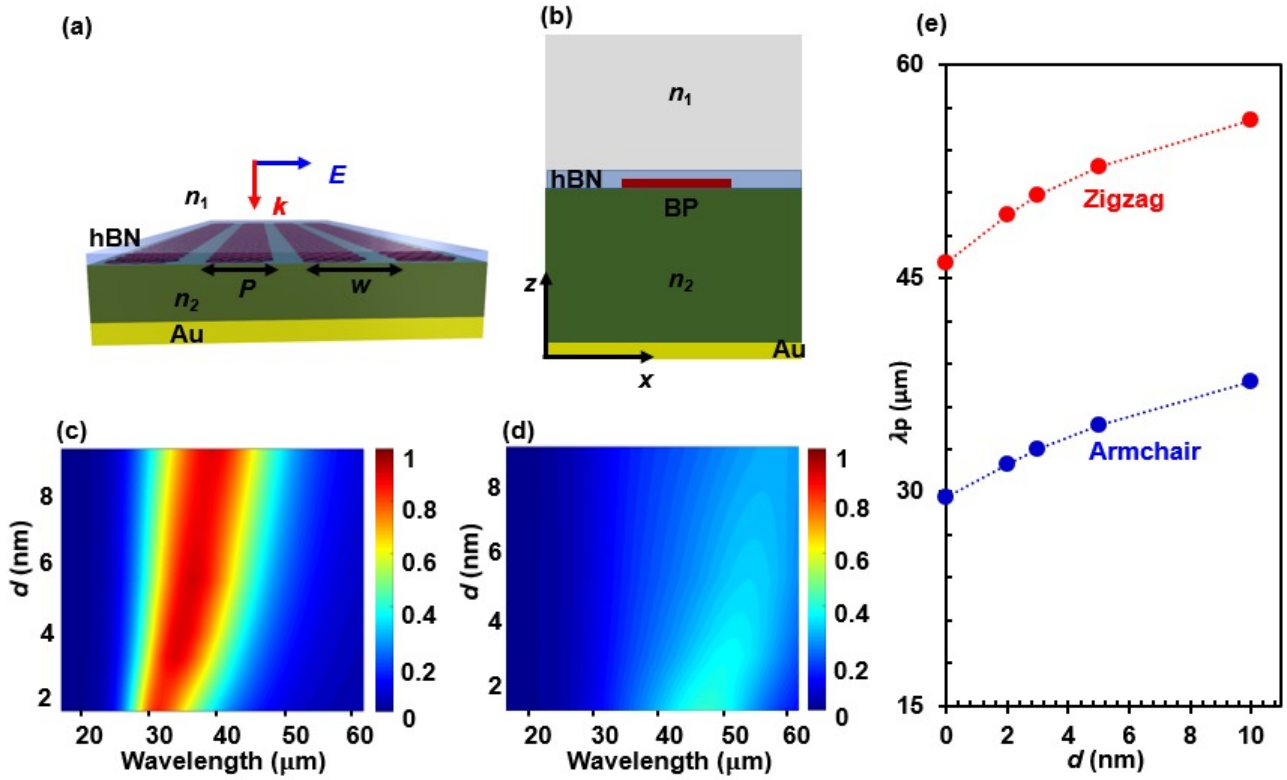

Fig. 4: **(a)** 3D and **(b)** 2D schematics of periodic phosphorene nanoribbons enclosed by a hBN layer of thickness *d*. The optical response is shown for the **(c)** armchair and (d) zigzag directions **(e)** Normal incidence TM mode electric field absorption response for different hBN thicknesses, *d* (nm) shown for both armchair and zigzag polarization directions. Here, w = 225 nm, n_2= 1.71, n_1= 1.0, N = 2.5 x 10^{13}cm^{-2}, and P = 250nm.

We also studied the case of a large ribbon width, w = 225 nm, to reduce the gap between successive ribbons for N = 2.5 x 10^{13}cm^{-2}. We observe resonant wavelength shifts in the armchair polarization direction from about 29 to 39μm as well as 47 to 56 μm along the zigzag direction. Absorption strength is maintained at about 80-90% in the armchair direction while absorption peak intensity gradually drops as the thickness increases in the zigzag direction. We also notice a broadening of the absorption intensity along both directions. While the introduction of the hBN protective layer is seen to enhance strong field localization along the armchair direction, it resulted in weak field confinements along the zig-zag direction.

6. CONCLUSION

We have investigated the tunable absorption capabilities of black phosphorous nanoribbons as well as their edge-confined plasmonic characteristics within select dielectric environments. Analytical schemes of the plasmonic dispersive behaviors were reported to depend on BP anisotropy and surrounding dielectric environment. In particular, the SPP confinement factor, in addition to having a strong effect on isolated BP nanoribbons, was found to increase as the refractive index of the surrounding dielectric medium increases. We reveal that, by scaling the BP into nanoribbon sizes, it is possible to activate the formation of edge plasmons that give rise to enhanced absorption. Due in part to the anisotropic nature of BP, we show that information regarding spectral positions and absorption peaks can be inherently modified by adjusting the electron density, refractive index, and ribbon size and spacing; these results also corroborate hypothesized theoretical formulations[43]. To address the challenge posed by the possibility of degradation through oxidation, a protective nanolayer of hBN metamaterial was introduced to encapsulate the BP ribbons in the computation. The result promotes the possibility of obtaining desired resonance modes that span the infrared range and extends our understanding of BP plasmons.

REFERENCES

1. Law, S., Yu, L., Rosenberg, A. & Wasserman, D. All-semiconductor plasmonic nanoantennas for infrared sensing. *Nano Lett.* **13**, 4569–4574 (2013).
2. Atwater, H. A. The Promise of Plasmonics. *Scientific American* **296**, 56–63 (2007).
3. Pendry, J. B., Schurig, D. & Smith, D. R. Controlling electromagnetic fields. *Science* **312**, 1780 (2006).
4. Fei, Z. *et al*. Gate-tuning of graphene plasmons revealed by infrared nano-imaging. *Nature* **487**, 82–85 (2012).
5. Yan, H. *et al*. Infrared spectroscopy of tunable Dirac terahertz magneto-plasmons in graphene. *Nano Lett.* **12**, 3766–3771 (2012).
6. Fang, Z. *et al*. Active tunable absorption enhancement with graphene nanodisk arrays. *Nano Lett.* **14**, 299–304 (2014).
7. Yan, H. *et al*. Damping pathways of mid-infrared plasmons in graphene nanostructures. *Nat. Photonics* **7**, 394–399 (2013).
8. Li, L. *et al*. Black phosphorus field-effect transistors. *Nat. Nanotechnology* **9**, 372–377 (2014).
9. Xia, F., Wang, H. & Jia, Y. Rediscovering black phosphorus as an anisotropic layered material for optoelectronics and electronics. *Nature Commun.* **5**, 4458 (2014).
10. Liu, H. *et al*. Phosphorene: an unexplored 2D semiconductor with a high hole mobility. *ACS Nano* **8**, 4033–41 (2014).
11. Wang, X. *et al*. Highly anisotropic and robust excitons in monolayer black phosphorus. *Nat. Nanotechnology* **10**, 517–521 (2015).
12. Koenig, S., Doganov, R., Schmidt, H., Castro Neto, A. & Ozyilmaz, B. Electric field effect in ultrathin black phosphorus. *Appl. Phys. Lett.* **104**, 103106 (2014).
13. Qiao, J., Kong, X., Hu, Z., Yang, F. & Ji, W. High-mobility transport anisotropy and linear dichroism in few-layer black phosphorus. *Nat. Commun.* **5**, 4475 (2014)
14. Low, T. *et al*. Plasmons and Screening in Monolayer and Multilayer Black Phosphorus. *Phys. Rev. Lett.* **113**, 106802 (2014).
15. Rodin, A. S. & Castro Neto, A. H. Collective modes in anisotropic double-layer systems. *Phys. Rev. B* **9**, 075422 (2015).
16. Liu, Z. & Aydin, K. Localized surface plasmons in nanostructured monolayer black phosphorus. *Nano Letters* **16**(6), 3457–3462 (2016).
17. Jiang, Y., Roldán, R., Guinea, F. & Low, T. Magneto-electronic properties of multilayer black phosphorus. *Phys. Rev. B* **92**, 085408 (2015).
18. Jin, F., Roldán, R., Katsnelson, M. I. & Yuan, S. Plasmonics in strained monolayer black phosphorus. *Phys. Rev. B* **92**, 115440 (2015).
19. Rodin, A. S., Carvalho, A. & Castro Neto, A. H. Strain-induced gap modification in black phosphorus. *Phys. Rev. Lett.* **112**, 17680 (2014).
20. Yang, J. *et al*. Optical tuning of exciton and trion emissions in monolayer phosphorene. *Light: Sci. Appl.* **4**, e312 (2015).
21. Li, P. & Appelbaum, I. Electrons and holes in phosphorene. *Phys. Rev. B* **90**, 115439 (2014).
22. Engel, M., Steiner, M. & Avouris, P. Black Phosphorus Photodetector for Multispectral, High-Resolution Imaging. *Nano Lett.* **14**, 6414–6417 (2014).
23. Viti, L. *et al*. Black phosphorus terahertz photodetectors. *Adv. Mater.* **27**, 5567–5572 (2015).
24. Castellanos-Gomez, A. *et al*. Isolation and characterization of few-layer black phosphorus. *2D Materials* **1**, 025001 (2014).
25. Buscema, M. *et al*. Fast and broadband photoresponse of few-layer black phosphorus field-effect transistors. *Nano Lett.* **14**, 3347–3352 (2014).
26. Ziletti, A., Carvalho, A., Campbell, D. K., Coker, D. F. & Castro Neto, A. H. Oxygen defects in phosphorene. *Phys. Rev. Lett.* **114**, 046801 (2015).
27. Favron, A. *et al*. Exfoliating pristine black phosphorus down to the monolayer: photo-oxidation and electronic confinement effects. *arXiv preprint arXiv:1408.0345* (2014).
28. Sland, J. O., Steele, G. A., van der Zant, H. S. & Castellanos-Gomez, A. Environmental instability of few-layer black phosphorus. *2D Mater.* **2**, 011002 (2015).
29. Kim, J. S. *et al*. Toward air-stable multilayer phosphorene thin-films and transistors. *Sci. Rep.* **5**, 8989 (2015).
30. Pei, J. *et al*. Producing air-stable monolayers of phosphorene and their defect engineering. *Nat. Commun.* **7**, 10450 (2016).

31. Asahina, H. & Morita, A. Band structure and optical properties of black phosphorus. *Journal of Physics C: Solid State Physics* **17**, 1839 (1984).
32. Low, T. *et al*. Tunable optical properties of multilayer black phosphorus thin films. *Phys. Rev. B* **90**, 075434 (2014).
33. Palik, E. D. Handbook of Optical Constants. Academic Press Inc., San Diego (1985).
34. COMSOL Multiphysics, v. 5.0. www.comsol.com. COMSOL AB, Stockholm, Sweden.
35. Thongrattanasiri, S., Koppens, F. H. & de Abajo, F. J. G. Complete optical absorption in periodically patterned graphene. *Phys. Rev. Lett.* **108**, 047401 (2012).
36. Engel, M. *et al*. Light-matter interaction in a microcavity-controlled graphene transistor. *Nat. Commun.* **3**, 906 (2012).
37. Li, H. H. Refractive index of alkali halides and its wavelength and temperature derivatives. *J. Phys. Chem. Ref. Data* **5**, 329–528 (1976).
38. Maharana, P. K., Jha, R. & Palei, S. Sensitivity enhancement by air mediated graphene multilayer based surface plasmon resonance biosensor for near infrared. *Sens. Actuators. B: Chem.* **190**, 494–501 (2014). pp.
39. Velizhanin, K. A. Geometric universality of plasmon modes in graphene nanoribbon arrays. *Phys. Rev. B: Condens. Matter Mater. Phys.* **91**, 125429 (2015).
40. Brar, V. W., Jang, M. S., Sherrott, M., Lopez, J. J. & Atwater, H. A. Highly confined tunable mid-infrared plasmonics in graphene nanoresonators. *Nano Lett.* **13**, 2541–2547 (2013).
41. Viti, L. *et al*. Heterostructured hBN-BP-hBN Nanodetectors at Terahertz Frequencies. *Adv. Mater.* **28**, 7390–7396 (2016).
42. Chen, X. *et al*. High-quality sandwiched black phosphorus heterostructure and its quantum oscillations. *Nat. Commun.* **6**, 7315 (2015).
43. Debu, D. T et al., Tuning Infrared Plasmon Resonance of Black Phosphorene Nanoribbon with a Dielectric Interface, *Scientific Reports*, Article vol. 8, p. 10, (2018)